ENERGY DEPOSITION IN THE SECTOR 37 SCRAPER OF THE ADVANCED PHOTON SOURCE STORAGE RING*

J. C. Dooling†, M. Borland, Y. C. Chae, and R. Lindberg, ANL, Argonne, IL 60439, USA

Abstract

The horizontal scraper in the sector 37 straight section of the Advanced Photon Source storage ring serves as a diagnostic to probe both the edge of the beam as well as the physical aperture when the store is lost. Initially, the scraper was meant only to be a diagnostic; high-density, short-radiation-length material used in the device was intended to stop halo, not the full beam. Damage to this device was recently discovered, and as a result, we began an effort to model and improve the scraper. Modeling with `elegant` provides loss distributions for several scenarios such as muting one or both rf systems in combination with firing injection kickers. The loss distributions are used as input to a MARS model of the scraper. Beam dumps from 100 mA dissipate a total of 2600 J. Most of this energy is not deposited locally; however, depending on the geometry and physical make-up, sufficient power density exists to damage the device on beam-facing surfaces. Testing is currently planned to examine the suitability of different beam-facing materials. Because of non-local energy deposition, we are evaluating the secondary role for this scraper as a spoiler rather than a beam dump.

INITIAL DAMAGE AND TESTING

During the Spring 2011 APS shutdown, damage to the sector 37 (S37) scraper was observed, and the device was removed from the storage ring (SR). A photograph of the damaged region is presented in Figure 1; the view is looking downstream. The thickness of the W is 2.54 cm. The

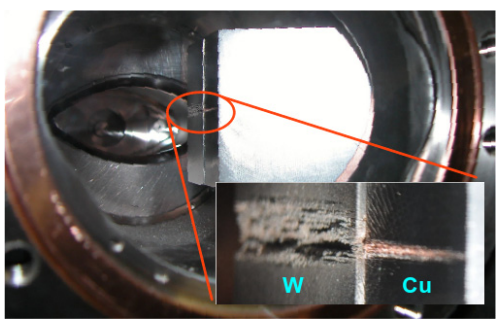

Figure 1: S37 scraper after removal from the SR in April 2011. View is looking downstream.

S37 scraper shown in Fig. 1 had been in use for seven years. The scraper was rebuilt using the same geometery and materials with the intention of employing the device only for diagnostics and collimation while a new design was considered. The rebuilt scaper was reinstalled in the SR in January 2012. Because of installation issues, the device was not used until the final day of the Spring 2012 run when beam dump studies were carried out. After shutdown the device was removed from the SR. During the study, beam was purposely dumped on the scraper using both 24-bunch and hybrid fill patterns. An image of the tungsten region damaged by 24-bunch beam dumps is presented in Figure 2.

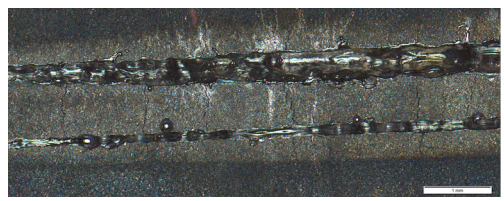

Figure 2: Tungsten region of the rebuilt S37 scraper after removal from the SR in May 2012. Beam motion: left to right.

SIMULATIONS

The particle-matter interaction program MARS [1] is used to estimate energy deposition within the scraper employing loss distributions generated with `elegant` [2]. The scraper components included in the MARS model that directly interact with the beam are shown in Figure 3; the beam travels from left to right. The tapered upstream portion is water-cooled copper. The downstream part is composed of scintered tungsten and is not directly water cooled.

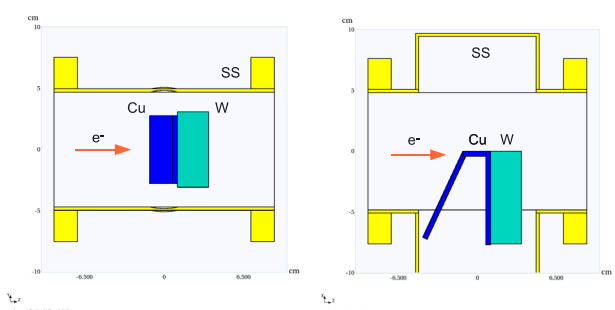

(a) y-z view, x=-1.1 cm (b) x-z view, y=0 cm

Figure 3: Sector 37 baseline scraper geometry modeled in MARS; a) an elevation view at the edge of the scraper (x=-1.1 cm) and b) a plan view at beam elevation (y=0).

The loss distribution is generated by `elegant` for a hy-

* Work supported by the U.S. Department of Energy, Office of Science, under contract number DE-AC02-06CH11357.

† jcdooling@anl.gov

ISBN 978-3-95450-138-0

brid fill pattern; the distribution includes beam loading effects and quantum fluctuations [3]. These simulations allow us to test different beam loss scenarios, such as muting one or both rf systems or firing injection kickers after beam dump conditions have been detected. Phase-space loss distribution histograms are presented in Figure 4. The distribution represents the complete loss of 368 nC of circulating SR charge (100 mA) and is simulated with 10^5-10^6 trajectories.

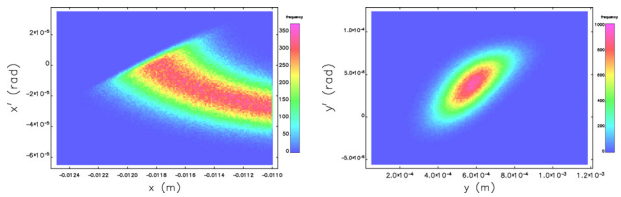

(a) horizontal phase-space, x-x' (b) vertical phase-space, y-y'

Figure 4: Phase-space loss distributions on the S37 scraper generated by `elegant`. The pixel sizes are 10 μm and 1 μrad.

Electron/positron fluence distributions are shown in Figure 5 for the geometry presented in Fig. 3. To determine the

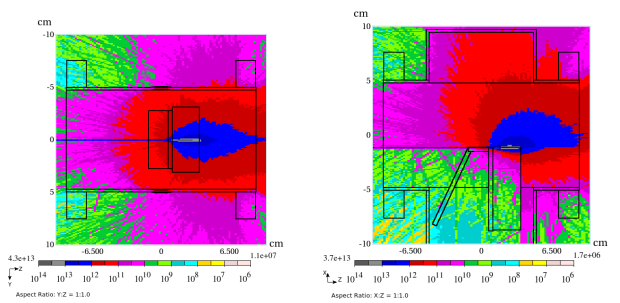

(a) y-z view, x=-1.1 cm (b) x-z view, y=0 cm

Figure 5: Electron/positron fluence in the Sector 37 baseline scraper geometry modeled in MARS. The two distributions overlay the geometry presented in Fig. 3.

stress on scraper material struck by the lost beam, we need to know the local energy deposition. For MARS simulations, the upstream copper portion of the scraper is divided into five equal-depth regions (Δz=0.357 cm). The tungsten is divided into seven regions, the first six with the same Δz and seventh with 1.1 mm added to make the total W-depth 2.54 cm. Peak dose and resultant temperature rise calculations are presented in Figure 6 assuming 100 mA (368 nC) are circulating in the SR in a hybrid-mode fill pattern. In Fig. 6, the change in temperature is calculated using Eq.(1) assuming all deposited energy appears instantaneously; this assumption ignores diffusion, which will be discussed below. Also, Fig. 6 shows the effect of firing one of the SR injection kickers after a dump has been detected. While firing kickers reduces the temperature increase significantly, it would not be sufficient to prevent melting.

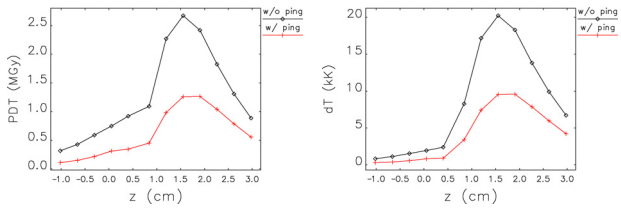

(a) total deposited dose (PDT) (b) instantaneous temperature rise

Figure 6: Absorbed dose and instantaneous temperature excursions.

ANALYSIS

Energy deposition is provided by MARS dose distributions. The instantaneous temperature rise in a given volume element can be calculated from MARS dose distributions, assuming that no heat transfer occurs over the period of energy deposition. Temperature rise due to an absorbed dose D_{ab} is

$$\Delta T = \frac{D_{ab} A_w}{C_v}, \quad (1)$$

where A_w is the atomic weight, and C_v is the molar heat capacity. According to the Law of Dulong and Petit, $C_v = \frac{\partial}{\partial T}(3k_B T N_A) = 3k_B N_A = 24.94$ J K^{-1}mole^{-1}, where k_B is Boltzmann's constant; most metals differ only slightly from this value. The actual values of C_v for Cu and W are 24.44 J K^{-1} mole^{-1} and 24.27 J K^{-1} mole^{-1}.

The temperature rise given by Eq.(1) assumes that the energy deposition given by MARS occurs at a single instant in time. In a real loss event, however, electrons are lost over several turns, and diffusive/dissipative mechanisms may play a role in reducing the temperature change ΔT. We have analytically estimated the effect of heat diffusion using the axially symmetric Green function solution to the diffusion equation. While this simplified model neglects other factors affecting heat transport, our primary goal was to determine if diffusion might dramatically change the temperature rise predicted in Fig. 6(b). According to our calculations, simple diffusion can reduce the temperature by 40%-60% in 24-bunch mode and between 60% and 80% in hybrid mode. Hence, while diffusion is not neglible, it does not appear to provide significant temperature reductions. Interestingly, scraper damage was more prominant for the 24-bunch-mode beam loss, which qualititively agrees with the diffusion mode predictions.

MATERIAL ASSESSMENT

Our purpose is to safely dump the circulating charge in the SR in case of a machine protection system (MPS) trip or some other sudden beam loss event. Presently, the preferred method is to passively absorb the beam in a scraper that also acts as a beam dump.

We address the choice of appropriate scraper material by considering the ratio of thermal stress to yield stress for a given heat load [4]. At the same time, we recognize that the

heat load for a given irradiation also depends on the material chosen. Material properties affect heat loading because bremsstrahlung is the primary energy loss mechanism for high-energy electrons. The generation of bremsstrahlung radiation is roughly proportional to ρZ^2, where ρ and Z are the density and atomic number of the exposed material, respectively. In addition, our design must live within an allowable footprint in the existing SR.

Thermal stress may be expressed as

$$\sigma_T = E_Y \alpha \Delta T, \tag{2}$$

where E_Y is Young's Modulus of Elasticity, α is the thermal coefficient of expansion, and ΔT is the temperature rise defined in Eq.(1). We define the thermal stress parameter g as

$$g = \frac{E_Y \alpha \Delta T}{\sigma_y}, \tag{3}$$

where σ_y is the yield stress. The stress parameter can be written as

$$\begin{aligned} g &= \frac{E_Y \alpha E_T A_w}{\sigma_y C_{mol} \rho V} \\ &= \frac{E_Y \alpha A_w}{\sigma_y C_{mol}} k_B S_{pc} \frac{N_e}{\pi r_b^2}, \end{aligned} \tag{4}$$

where E_T is the total deposited energy, ρ is the density, V is the volume, k_B is Boltzmann's constant, S_{pc} is the collisional stopping power [5], and r_b is the radius of the beam. We assume the lost charge is uniformly distributed within r_b. In Eq.(4) we used the thin target approximation [6] $E_T \approx \frac{S_{pc}}{S_{pr}} N_e W_o \frac{\rho}{X_o} \Delta z$; also, $S_{pr} = \frac{W_o}{X_o}$, and $V = \pi r_b^2 \Delta z$. S_{pr} is the radiative stopping power, W_o is the electron energy, and X_o is the radiation length.

In Eq. (4), we have separated the material-related terms from the beam terms. S_{pc} is a function of both but varies slowly with atomic weight at 7 GeV. In Table 1, the g-ratio is calculated for several materials assuming $N_e = 2.3 \times 10^{12}$ and $r_b = 0.1$ mm.

Table 1: Material Properties and Thermal-to-Yield Stress Ratio. PG and PB represent pyrolytic graphite and polybutene 1300; both are assumed to be composed entirely of carbon.

Mat.	E_Y (GPa)	$\alpha \times 10^6$ (K^{-1})	C_{mol} $\left(\frac{J}{mole\text{-}K}\right)$	σ_y (MPa)	g
Be	248	12.4	16.44	345	11.6
PG	20.7	0.5	8.28	82.7	0.48
PB	6.9	4	10.08	37.9	2.30
Al	69	25	24.20	310	15.8
Ti	116	8.5	25.06	951	4.72
Cu	110	16.5	24.44	220	49.6
W	345	14.4	24.27	1510	49.6

Table 1 indicates only pyrolytic graphite exhibits a g-ratio less than 1; whereas, copper and tungsten show the largest g. The g-ratio for titanium, though relatively high, is still an order of magnitude lower than for copper. We note that based on the results in Table 1, one might conclude that copper and tungsten should suffer roughly equal damage; however, from direct observations, we know this not the case. In the actual scraper, the damage to the W block was much more severe than to the Cu one due in large part to the shorter radiation length and higher density in the W. Part of this difference may also be due to a horizontal offset in the tungsten that had its outboard surface 0.8 mm closer to the beam than that of the copper surface.

DISCUSSION

In the case of a 24-bunch beam dump, peak power densities are on the order of 10^{15}Wcm^{-2}. Fast beam loss diagnostics [7] indicate that shorter dumps usually found with 24-bunch fill patterns are more destructive. Using higher-melting-temperature, lower-Z materials while moving the beam with a kicker should increase the scraper damage threshold. Work is now underway to build a new scraper that will reduce both impedance and the generation of higher-order cavity modes. Of the 2600 J stored in the beam, only 760 J are deposited in the scraper after 1.24 X_o and 7.26 X_o of Cu and W, respectively. Reducing the scraper length in terms of X_o means the device will absorb even less energy and act more as a spoiler. Simulations of this approach show promise both in terms of survival of the spoiler and protection of downstream insertion devices.

ACKNOWLEDGMENT

Thanks to R. Soliday for assistance with data analysis scripts.

REFERENCES

[1] N.V. Mokhov, "The Mars Code System User's Guide," Fermilab-FN-628 (1995); http://www-ap.fnal.gov/MARS/; N.V. Mokhov, S.I. Striganov, "MARS15 Overview," AIP Conf. Proc. 896, pp. 50-60 (2007).

[2] M. Borland, Advanced Photon Source ANL/APS/LS-287 (2000).

[3] M. Borland, private communication, September 2011.

[4] D. Walz, private communication, June 2011.

[5] M. J. Berger et al., "Stopping powers for electrons and positrons," ICRU Report 37 ICRU, Washington, DC, 1984; http://physics.nist.gov/PhysRefData/Star/Text/intro.html

[6] R. H. Thomas et al., *Radiation Protection for Particle Accelerator Facilities*, NCRP Report 144, National Council on Radiation and Protection and Measurements, Bethesda, MD, 2003, p. 44 (2003).

[7] J. C. Dooling and M. Borland, "Simulation and Measurement of Beam Loss in the Narrow-Gap Undulator Straight Section of the Advanced Photon Source Storage Ring," IPAC'12, New Orleans, MOEPPB013, p. 107 (2012); http://www.JACoW.org

ISBN 978-3-95450-138-0